Mechanism of the Decomposition of Aqueous Hydrogen Peroxide over Heterogeneous TiSBA15 and TS-1 Selective Oxidation Catalysts: Insights from Spectroscopic and Density Functional Th...

5 AUTHORS, INCLUDING:

Xinzheng Yang
Chinese Academy of Sciences
58 PUBLICATIONS   984 CITATIONS

Mechanism of the Decomposition of Aqueous Hydrogen Peroxide over Heterogeneous TiSBA15 and TS-1 Selective Oxidation Catalysts: Insights from Spectroscopic and Density Functional Theory Studies

Chang Won Yoon,[†,⊥] Kurt F. Hirsekorn,[§] Michael L. Neidig,[§,∥] Xinzheng Yang,[†] and T. Don Tilley*,[†,‡]

[†]Department of Chemistry, University of California, Berkeley, California 94720, United States

[‡]Chemical Sciences Division, Lawrence Berkeley National Laboratory, 1 Cyclotron Road, Berkeley, California 94720, United States

[§]Core R&D-Chemistry and Catalysis, The Dow Chemical Company, Midland, Michigan 48674, United States

Ⓢ *Supporting Information*

ABSTRACT: The Ti-based heterogeneous catalysts **TiSBA15**, **Bu$_{cap}$TiSBA15**, **TS-1**, and **[Ti,Al]-MFI** were investigated with respect to controlling factors for the competitive decomposition of aqueous H_2O_2 during selective catalytic oxidations. DRUV−vis spectroscopy revealed that the titanium species in these materials exist mainly in isolated, tetrahedral coordination environments. The observed rates of H_2O_2 decomposition at 65 °C in acetonitrile decreased in the following order: **Bu$_{cap}$TiSBA15** > **TiSBA15** and **TS-1** > **[Ti,Al]-MFI**. The decompositions of H_2O_2 were also monitored in the presence of inorganic additives and Brønsted acids and bases, in benzene/aqueous biphasic solutions. Significant retardation of the decomposition rates with the KH_2PO_4 additive was found with **TiSBA15**, which suggests that the

Possible H_2O_2 decomposition pathways

KH_2PO_4 stabilizer may be useful for optimization of hydrogen peroxide efficiency in catalytic oxidations. DRUV−vis spectroscopy was employed to identify possible catalytically active intermediates, proposed to be Ti(IV)(OOH) species that are produced upon reaction of the Ti-based materials and H_2O_2. Density Functional Theory (DFT) studies starting from a molecular model, $(HO)Ti[OSi(OH)_3]_3$, suggest that three Ti(IV)(OOH) intermediates are in equilibrium, and the formation of Ti−O$^•$ and HOO$^•$ radical species may be involved in the H_2O_2 decomposition. In addition, the potential role of KH_2PO_4 in the H_2O_2 decomposition process, as a proton acceptor in a $[Ti(OO)(HOP(O)(OH)_2)]$ complex, has been investigated.

KEYWORDS: heterogeneous catalysts, titanium, SBA15, hydrogen peroxide, decomposition, mechanism, green process
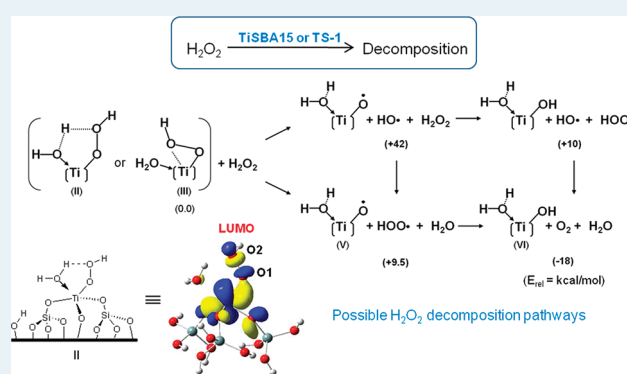
■ INTRODUCTION

Catalytic oxidations over heterogeneous catalysts play an important role in industrial chemical processes. Such reactions cover a wide range of substrates and oxidizing agents, though the latter often generate environmentally hazardous waste streams.[1] Thus, the development of innovative technologies that utilize benign oxidants (e.g., H_2O_2 and O_2) can significantly contribute to the reduction of chemical wastes. Considerable attention has focused on utilization of H_2O_2 as an attractive, alternative oxidant for existing industrial processes, particularly given its advantages of (1) a high content of active oxygen (47 wt %), and (2) the release of only H_2O as a byproduct.[2] In this context, a wide range of transition metal-based catalysts (e.g., V, Ti, Mn, Fe, Cu, and Mo) for H_2O_2 oxidation reactions have been investigated.[3] While activations of H_2O_2 are considerably more facile than those associated with molecular oxygen, making it a kinetically attractive oxidant, this reagent originates from the partial reduction of molecular oxygen with valuable hydrogen. Thus, high H_2O_2 efficiencies (defined as the ratio of moles of product to moles of hydrogen peroxide consumed) are typically

required for economically viable processes, and efforts should focus on the inhibition of competitive H_2O_2 decomposition pathways.[4] In addition, a complementary understanding of the mechanisms differentiating the desired hydrocarbon oxidation from the undesired H_2O_2 decomposition is required.

Owing to their established performance as heterogeneous oxidation catalysts for organic substrates, Ti-based materials that utilize aqueous H_2O_2 have been widely investigated[5] and should serve as useful systems for studies to gain mechanistic understanding. In particular, titanosilicate-1 (**TS-1**) has been shown to catalyze the epoxidation of propylene to propylene oxide,[6] and the oxidation of benzene to phenol[7−10] using H_2O_2 as the oxidant. In addition, it has been demonstrated that site-isolated **TiSBA15** materials obtained by the thermolytic molecular precursor (TMP) method efficiently epoxidize cyclohexene with H_2O_2, and further surface and active-site modifications of the **TiSBA15** material with (N,N-dimethylamino)butyldimethylsilane,

BuMe$_2$SiNMe$_2$, have resulted in a drastically improved catalyst for this reaction.[11−13] The catalytic performance of a Ti-containing polyoxometallate, $[PTi(OH)W_{11}O_{39}]^{4−}$ has also been demonstrated for the oxidation of alkenes, thioethers, and alkylphenols with aqueous H_2O_2.[14] More recently, titanium silsesquioxane complexes in a polydimethylsiloxane membrane have exhibited high epoxide selectivity as well as H_2O_2 selectivity in the epoxidation of cyclohexene and 1-octene.[15]

Despite these advances, a significant remaining challenge for application of Ti-based catalysts concerns the efficiency of H_2O_2 utilization in oxidation reactions.[16] Thus, a detailed understanding of the mechanisms for catalytic oxidation, and for the competing hydrogen peroxide decomposition, at a supported titanium center is highly desired. The mechanism for the epoxidation of olefins by H_2O_2, as catalyzed by **TS-1** and related materials, has been investigated by experimental and computational methods. On the basis of Diffuse Reflectance UV−visible (DRUV−vis) spectroscopy, Extended X-ray Absorption Fine Structure (EXAFS), X-ray Absorption Near Edge Structure (XANES), and Density Functional Theory (DFT) methods, both Ti(η^1-OOH) and Ti(η^2-OOH) species have been proposed as active intermediates.[17] However, there is still uncertainty regarding the role of such species in specific oxidation reactions. In addition, despite the numerous studies on possible oxidation mechanisms for Ti-based catalysts, few mechanistic studies have addressed the mechanism of H_2O_2 decomposition at such catalytic centers.[18−20]

In this contribution, we describe governing factors for the decomposition of H_2O_2 over commonly employed types of Ti-based, site-isolated heterogeneous catalysts, mesoporous **TiSBA15**[21] and **Bu$_{cap}$TiSBA15**,[11] and microporous **TS-1**[22,23] and **[Ti,Al]-MFI**.[24] These studies demonstrate that surface acidity of the catalysts and the solution pH play a critical role in the degradation of H_2O_2. In addition, inorganic additives can influence the decomposition of H_2O_2 by interacting with catalytically active Ti sites, and in particular, a phosphate additive (KH_2PO_4) efficiently suppresses the decomposition. On the basis of diffuse reflectance UV−vis (DRUV) spectroscopic studies and DFT methods, it is proposed that titanium hydroperoxo intermediates decompose H_2O_2 by oxidation, via formation of Ti−O$^\bullet$ and hydroperoxo radical (HOO$^\bullet$) species. Furthermore, phosphate monobasic (KH_2PO_4) has been identified as an additive that suppresses H_2O_2 decomposition over **TiSBA15**, possibly by its binding mode to the surface-bound titanium hydroperoxy complex.

■ RESULTS

Material Synthesis and Characterization. The mesoporous silica SBA15[25] and Ti(O^{i}Pr)[OSi(O^{i}Bu)$_3$]$_3$[26,27] were prepared according to literature procedures. Grafting of Ti(O^{i}Pr)[OSi-(O^{i}Bu)$_3$]$_3$ onto the surface of SBA15, followed by calcination at 250 °C under O$_2$, afforded 10 g of **TiSBA15** catalyst[21] with 2.69 Ti wt % as determined by inductively coupled plasma (ICP) atomic emission spectroscopy. The surface silanol and titanol sites were then silylated by treatment of the dried **TiSBA15** material with excess (N,N-dimethylamino)dimethylbutylsilane (Me$_2$N-SiMe$_2$Bu) in hexane, to generate a **Bu$_{cap}$TiSBA15** material.[21] The Ti content in **Bu$_{cap}$TiSBA15** was determined to be 1.53 wt % by ICP analysis and was lower than that in **TiSBAS15**, as expected. The microporous materials **TS-1** and **[Ti, Al]-MFI** possessed 1.08 and 1.05 wt % Ti contents, respectively,

as determined by ICP emission spectroscopy following complete digestion in nitric acid.

Nitrogen porosimetry was employed to measure the surface area and pore structure of the materials. The N$_2$ adsorption−desorption data for **TiSBA15** and **Bu$_{cap}$TiSBA15** exhibited type IV isotherms indicative of mesoporous materials with narrow pore size distributions (Supporting Information, Figure S1). The parent **TiSBA15** material was found to have a Brunauer−Emmett−Teller (BET) surface area of 555 m^2 g$^{−1}$ and a pore volume of 0.534 mL g$^{−1}$. Upon surface modification, the surface area and pore volume (of **Bu$_{cap}$TiSBA15**) decreased to 230 m^2 g$^{−1}$ and 0.366 mL g$^{−1}$, respectively. Thermogravimetric analysis (TGA) of **TiSBA15** revealed a 9.3% mass loss upon heating from room temperature to 1000 °C, attributed to surface-bound water on the materials. After the surface modification, a greater mass loss (13%) was observed under the same conditions (Supporting Information, Figure S2) because of the presence of the capping groups. The degree of −OH site capping by silyl groups in **Bu$_{cap}$TiSBA15** was determined by titration of the OH sites on the surface of the materials. Reactions[28] of the materials with Mg(CH$_2$Ph)$_2$(THF)$_2$ were monitored by ^{1}H NMR spectroscopy. The OH coverage for **TiSBA15** was determined to be 1.9 OH/nm^2 whereas that of **Bu$_{cap}$TiSBA15** was 0.16 OH/nm^2, indicating that most of the Brønsted acidic sites in **Bu$_{cap}$TiSBA15** are blocked by the silyl capping groups. The hygroscopic natures of **TiSBA15** and **Bu$_{cap}$TiSBA15** were examined by placing both catalysts in a sealed container with a humid atmosphere at room temperature for 50.5 h, followed by analyses with TGA and differential thermal analysis (DTA). The unmodified **TiSBA15** material exhibits a H$_2$O loss of about 25% below 80 °C with a H$_2$O desorption temperature of 48 °C, measured as the minimum of the endothermic transition corresponding to water loss, whereas the modified **Bu$_{cap}$TiSBA15** material exhibits almost no H$_2$O loss below 100 °C, confirming the hydrophobic nature of this material (Supporting Information, Figure S3). The BET surface areas, pore radii, OH site densities, and TGA data for **TiSBA15** and **Bu$_{cap}$TiSBA15** are in good agreement with those previously reported, as summarized in Supporting Information, Table S1.

DRUV−vis spectroscopy was employed to identify the local structure of the as-synthesized, supported Ti(IV) centers. As depicted in Supporting Information, Figure S4 (blue line), the DRUV−vis spectrum of **TiSBA15** exhibited a sharp absorption band centered at 214 nm (O$^{2−}$ → Ti^{4+} ligand-to-metal charge-transfer) indicative of site-isolated tetrahedral Ti(IV) centers. **Bu$_{cap}$TiSBA15** also displayed a narrow single band centered at 214 nm (Supporting Information, Figure S4; red line), indicating that the single-site tetrahedral Ti(IV) centers are unchanged after the surface modification. The zeolitic materials **TS-1** and **[Ti,Al]-MFI** exhibit similar spectral features that indicate the presence of tetrahedral Ti centers (Supporting Information, Figure S5).

Influence of Surface Modification on H$_2$O$_2$ Decomposition. The relative rates of H$_2$O$_2$ decomposition over the Ti-based materials were determined by treatment of **TiSBA15**, **Bu$_{cap}$TiSBA15**, and **TS-1** (ca. 5 mg, 2.8 μmol Ti for **TiSBA15**) with homogeneous acetonitrile-d$_3$ (0.5 mL) solutions containing aqueous H$_2$O$_2$ (50 μL, 0.86 mmol, ca. 300 equiv relative to Ti for **TiSBA15**), and methylene chloride (5.0 μL) as an internal standard, followed by immersing the resulting mixture in a 65 °C oil bath. As depicted in Figure 1, the presence of the hydrophobic surface of **Bu$_{cap}$TiSBA15** results in a relatively sharp ^{1}H NMR
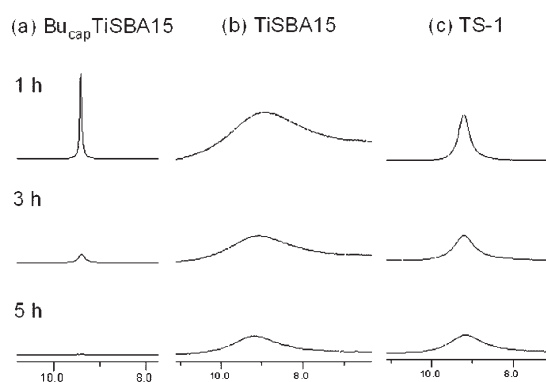
Figure 1. ^{1}H NMR spectra of mixtures containing hydrogen peroxide (50 μL), methylene chloride (5 μL), and acetonitrile-d_3 (0.5 mL) as a function of time in the presence of (a) **Bu$_{cap}$TiSBA15**, (b) **TiSBA15**, and (c) **TS-1**. The reaction temperature was 65 °C.
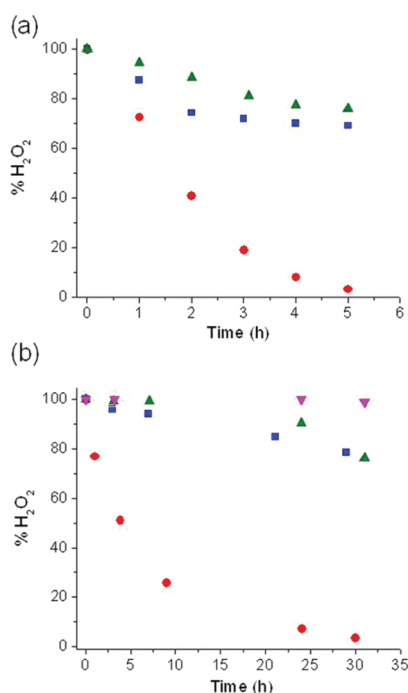

Figure 2. Plots of H$_2$O$_2$ decomposition at 65 °C from mixtures of hydrogen peroxide (aq), methylene chloride, and acetonitrile-d_3 over **TiSBA15** (blue solid squares), **Bu$_{cap}$TiSBSA15** (red solid circles), **TS-1** (green solid upward-pointing triangles), and **[Ti,Al]-MFI** (magenta solid downward-pointing triangles) as monitored by ^{1}H NMR spectroscopy: (a) In the absence of benzene, and (b) in the presence of benzene (1.6 mL).

resonance for H$_2$O$_2$ centered around δ = 9.3 ppm, while the hydrophilic **TiSBA15** gave rise to a broad H$_2$O$_2$ resonance at the same chemical shift. The rates of H$_2$O$_2$ decomposition decreased in the order **Bu$_{cap}$TiSBA15** > **TiSBA15** > **TS-1** (Figure 2a). The H$_2$O$_2$ proton resonances are very broad in the presence of **[Ti,Al]-MFI**, which made quantitative analyses difficult in aqueous/CD$_3$CN mixtures. The observed broadening may be associated with a higher affinity of the surface for H$_2$O$_2$, which could result in rapid proton exchange between surface hydroxyl groups and hydrogen peroxide.

Table 1. Decomposition of H$_2$O$_2$ over the Catalysts at 65 °C after 3 h

entry	additives[b]	initial pH	final pH	% decomposition
		TiSBA15[a]		
1	none	4−5	3	37
2	CF$_3$COOH	1	1	1.1
3	KHSO$_4$	1	1	2.3
4	KHF$_2$	3	4	2.2
5	Na$_2$SO$_4$	5	3−4	23.4
6	NaHCO$_3$	8−9	9	>98
7	K$_2$CO$_3$	12	12	>99
8	K$_3$PO$_4$	13	13	>99
9	K$_2$HPO$_4$	9	8	36
10	KH$_2$PO$_4$	4−5	4	6.5
		Bu$_{cap}$TiSBA15[a]		
11	none	4−5	3−4	12
12	CF$_3$COOH	1	1	1.1
13	KHF$_2$	3	3	2.2
14	K$_2$HPO$_4$	9	8	24
15	KH$_2$PO$_4$	4−5	3−4	8.9
		TS-1[a]		
16	none	4	4	1.1
17	K$_2$HPO$_4$	8−9	8	9.8
18	KH$_2$PO$_4$	4	4	5.8
19	Na$_2$SO$_4$	4	4−5	2.2
20	K$_2$CO$_3$	11	12	>95
		[Ti,Al]-MFI[a]		
21	none	4	3	3.2
22	K$_2$HPO$_4$	8−9	8	8.7
23	KH$_2$PO$_4$	4	4	3.3
24	Na$_2$SO$_4$	4	3	2.4
25	K$_2$CO$_3$	11	12	>97
		No Catalyst[a]		
26	H$_2$O	4−5	5	0
27	K$_2$HPO$_4$	9	9	7.7
28	KH$_2$PO$_4$	4−5	4	4.5
29	Na$_2$SO$_4$	4	4	1.2
30	NaHCO$_3$	8−9	10	>98
31	K$_2$CO$_3$	12	12	>99

[a] **1** (ca. 5 mg), **2** (ca. 8 mg), **3** (ca. 8 mg), and **4** (ca. 8 mg) were used. [b] Each additive (aq, 1 M, 3.2 mL) was used except CF$_3$COOH (aq, 0.1 M, 3.2 mL).

Changes in the H$_2$O$_2$ concentrations in the presence of the more hydrophobic solvent, benzene, were also monitored by ^{1}H NMR spectroscopy in acetonitrile-d_3. Figure 2b illustrates decomposition profiles for aqueous hydrogen peroxide over **TiS-BA15**, **Bu$_{cap}$TiSBA15**, **TS-1**, and **[Ti,Al]-MFI** as a function of time. In control experiments with either no catalyst or with SBA15, the concentration of H$_2$O$_2$ remained nearly unchanged throughout 5 h of heating at 65 °C. In contrast, reaction of H$_2$O$_2$ with **Bu$_{cap}$TiSBA15** resulted in a significantly increased rate of H$_2$O$_2$ decomposition, with about 40% of the initial H$_2$O$_2$ concentration being lost after only 2 h. The rate of decomposition in the presence of **TiSBA15** was slower than that with **Bu$_{cap}$TiS-BA15** under the same reaction conditions, and **TS-1** exhibited an

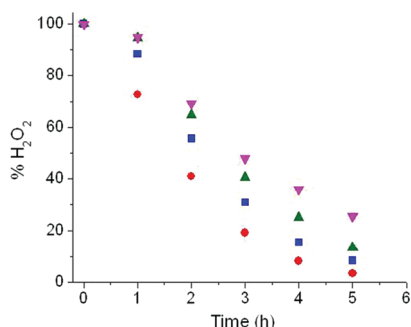**Figure 3.** H_2O_2 decompositions over **Bu_{cap}TiSBA15** at 65 °C in the presence of 2,6-di-*tert*-butyl-4-methylphenol (BHT): 0.0 mg (red solid circles), 2.0 mg (blue solid squares), 10 mg (green solid upward-pointing triangles), and 20 mg (magenta solid downward-pointing triangles).

even slower rate of decomposition. Among the materials used, **[Ti,Al]-MFI** displayed the slowest rate of H_2O_2 decomposition at 65 °C. Since essentially no decomposition was observed in the absence of the Ti-based catalysts, the Ti sites are assumed to be responsible for the H_2O_2 decomposition. Furthermore, the observed rates (**Bu_{cap}TiSBA15** > **TiSBA15** and **TS-1** > **[Ti, Al]-MFI**) appear to be related to the Brønsted acidity of the catalyst surface. **Bu_{cap}TiSBA15** possesses a very low surface coverage of acidic protons (OH density, $0.16/nm^2$), whereas **TiSBA15** exhibited an OH density of $1.9/nm^2$ on its surface. Moreover, because of the presence of the Al atoms, the surface hydroxyl groups of **[Ti,Al]-MFI** are more acidic than those of the **TS-1** material. Thus, it would appear that H_2O_2 is more stable under acidic conditions, as has been noted previously.[29] In all cases, the hydroxylation of benzene was negligible under the experimental conditions employed, as evidenced by ^{1}H NMR spectroscopy.

Influence of Additives on H_2O_2 Decomposition. Inorganic salts have been employed not only for suppressing the decomposition of H_2O_2,[30,31] but also for enhancing selectivity for a desired oxidation.[32−34] For example, buffer solutions of various salts (e.g., for the cations Na^+, K^+, and NH_4^+, and the anions phosphate, sulfate, and carbonate) were used to increase the selectivity for formation of propylene oxide.[34] In particular, inorganic salts represent promising peroxide stabilization agents that can act by adjusting the solution's acidity and/or by interacting directly with catalytic metal centers.

The influence of added Brønsted acids and bases on the H_2O_2 decomposition was investigated by addition of aqueous H_2O_2 (0.4 mL) to a benzene (1.6 mL)/aqueous (3.2 mL) biphasic solution containing the desired additives, followed by vigorous stirring of the resulting mixture at 65 °C for 3 h. As listed in Table 1, acids retarded the decomposition of H_2O_2, whereas bases had the opposite effect under the same reaction conditions. In the absence of additives, 37% of the initial H_2O_2 decomposed after 3 h (entry 1). However, with Brønsted acids the stabilization effects were significant, with only 1.1% of the initial H_2O_2 having decomposed after 3 h in the presence of CF_3COOH (entries 2 and 12). The $KHSO_4$ and KHF_2 additives also exhibited inhibitory effects on the degradations over **TiSBA15**, with about 98% of H_2O_2 being unchanged after 3 h at 65 °C (entries 3 and 4). A low degree of inhibition was observed in the presence Na_2SO_4 (entry 5, 23.4% decomposition). Degradation rates were drastically increased under basic conditions, and residual amounts of H_2O_2 were determined to be <1% after 3 h in the presence of K_2CO_3 (entries 7, 20, and 25) and K_3PO_4 (entry 8). It should be
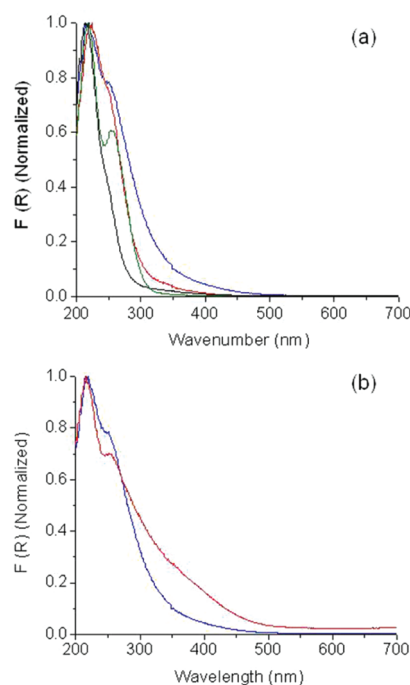

Figure 4. DRUV−vis spectra of **TiSBA15**: (a) Pure solids (black); after exposure in air (green); after reaction with anhydrous H_2O_2 (red), followed by drying; and after treatment with aqueous H_2O_2 (blue), followed by drying in vacuum. (b) Comparison after (blue) and before (red) drying in vacuum following addition of H_2O_2 (aq) to **TiSBA15**.

noted that the H_2O_2 decompositions occurred even in the absence of catalysts with the K_2CO_3 additive (entry 31). However, among the inorganic stabilizers which slightly raised solution acidity (pH 4−5; entries 1, 5, and 10), only the phosphate monobasic (KH_2PO_4) exhibited a significant inhibitory effect on decomposition over **TiSBA15** in the biphasic solution; that is, about 37% of H_2O_2 decomposed in 3 h in the absence of any additives (entry 1), while only 6.5% of H_2O_2 was lost in the presence of aqueous KH_2PO_4 solution (1 M, entry 10) under the same reaction conditions. Furthermore, the observed inhibition of H_2O_2 decomposition in the presence of KH_2PO_4 does not result purely from its Brønsted acidity. Thus, under slightly basic conditions (pH 8−9), K_2HPO_4 gave rise to slower decomposition (entry 9) with respect to that observed with $NaHCO_3$ as the additive (entry 6). The acidic additives ($pK_a < 2$) exhibited similar effects on the decompositions over **Bu_{cap}TiSBA15**, but for KH_2PO_4 a low degree of inhibition was found (entry 15). Note that because of its hydrophobic nature, **Bu_{cap}TiSBA15** was located at the benzene layer in the biphasic solutions. Thus, the low degree of inhibition in this case may result from slow diffusion of the anionic additive ($H_2PO_4^-$) to Ti sites in the benzene layer.

In contrast to the **TiSBA15** material, the influence of the KH_2PO_4 additive on the decompositions over **TS-1** and **[Ti,Al]-MFI** was less pronounced under the same reaction conditions. For example, 1.1 and 3.2% of the initial H_2O_2 decomposed in the absence of any additives (entries 16 and 21) while 5.8% and 3.3% of H_2O_2, respectively, degraded in the presence of the KH_2PO_4 salt (entries 18 and 23), indicating that the influence of the phosphate monoanion was not significant in these cases.

To examine whether radical species might play a role in the observed degradations of H_2O_2, mixtures containing H_2O_2 (50 μL), CH_2Cl_2 (5 μL), **Bu_{cap}TiSBA15** (ca. 5 mg, 1.6 μmol Ti),

and a radical trap, 2,6-di-*tert*-butyl-4-methylphenol (BHT; 2.0–20 mg, 5.7–57 equiv relative to Ti; 0.011–0.11 equiv relative to H_2O_2), were monitored by ^1H NMR spectroscopy. As displayed in Figure 3, the rate of H_2O_2 degradation decreased with an increasing amount of BHT at 65 °C in acetonitrile-d_3. Thus, it appears that radical species may play a role in the decomposition of H_2O_2 in aqueous solutions. A similar retardation of H_2O_2 decomposition was observed for the **TiSBA15** catalyst in the presence of BHT (Supporting Information, Figure S6).

Observation of Catalytically Relevant Intermediates. DRUV–vis spectroscopy was employed to investigate the formation of Ti-based intermediates during the H_2O_2 decompositions. The DRUV–vis spectrum of **TiSBA15** exhibits a sharp, single transition with λ_{max} = 214 nm (Figure 4a, black), indicative of site-isolated, tetrahedral environment around Ti.[34] Upon exposure of **TiSBA15** to air at room temperature for 3 days, a new shoulder centered at around 258 nm (Figure 4a, green) appeared, indicating hydration of the Ti centers to produce penta- and/or pseudo-octahedral environments for Ti.[35,36] The latter absorption disappeared upon drying of the wet **TiSBA15** material in an oven (140 °C, 20 h), indicating regeneration of the tetrahedral Ti sites in the material (Supporting Information, Figure S7). Upon addition of aqueous H_2O_2 to **TiSBA15**, an intense yellow color immediately appeared. The resulting **TiSBA15** material was isolated by filtration and dried under vacuum overnight. By DRUV–vis spectroscopy, this material exhibited an additional broad signal from 300 to 500 nm (Figure 4a, blue), assigned to Ti-OO(H) (Ti-OOH or Ti-η^2-O_2) species. When aqueous H_2O_2 was still in contact with the catalyst, this visible band was intense (Figure 4b, red), but became faint upon drying in vacuum (Figure 4b, blue). To help identify the broad signal centered between 300 to 500 nm, anhydrous H_2O_2,[37] prepared in methylene chloride-d_2 (Supporting Information, Figure S8), was allowed to react with **TiSBA15** at room temperature for 5 min. Removal of the solvent produced a nearly colorless solid that exhibited a DRUV–vis spectrum (Figure 4a, red) containing a shoulder at 261 nm, indicating expansion of the coordination sphere of the Ti site, for example, to $(H_2O)Ti(\eta^1$-OOH) and/or $(H_2O)Ti(\eta^2$-OOH) species. Analogously, reaction of **TiSBA15** with *tert*-butyl hydroperoxide (TBHP) in a decane/CH_3CN mixture at room temperature for 1 h afforded a Ti-OO^{t}Bu species that exhibits only a shoulder centered around 260 nm in the DRUV–vis spectrum (Supporting Information, Figure S9), indicating interaction of TBHP with the Ti centers to give penta- or pseudo-octahedral complexes. No visible bands were observed upon addition of H_2O to **TiSBA15** following the same procedure, nor upon addition of H_2O_2 to SBA15. The visible band from 300 to 500 nm is thus associated with both Ti-η^2-OO(H) and H_2O being present in the sample.

To investigate the role of the phosphate anion in inhibiting H_2O_2 decomposition, **TiSBA15** was treated with a H_3PO_4 (aq, 1M), KH_2PO_4 (aq, 1M), and K_2HPO_4 (aq, 1M) solutions at room temperature for 2 h, followed by drying in air for about 3 h. These procedures did not produce a color change. After treatment of **TiSBA15** with H_3PO_4, only a band centered at λ_{max} = 214 nm (similar to that of the untreated sample; Figure 4, black trace) was observed, but interestingly, **TiSBA15** treated with $H_2PO_4^-$ exhibited a broad absorption band from 250 to 350 nm with a shoulder (Figure 5, red trace), which may be attributed to the formation of Ti–O–P heterolinkages.[38] Solid-state ^{31}P magic-angle-spinning (MAS) NMR spectroscopy was employed to probe the nature of any new phosphorus containing species.
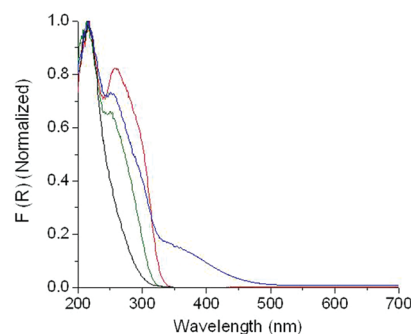

Figure 5. DRUV–vis spectra of **TiSBA15** after treatment with (a) H_3PO_4 (black), (b) K_2HPO_4 (green), (c) KH_2PO_4 (red), and (d) both KH_2PO_4 and H_2O_2 (blue).

Following treatment of **TiSBA15** with KH_2PO_4, a new species is indicated by a broad signal centered at δ = −2 ppm, which suggests the formation of Ti–O–P linkage. Note that the spectrum of solid KH_2PO_4 exhibits a single peak at δ = 4 ppm relative to an external standard H_3PO_4 (Supporting Information, Figure S10). Similarly, **TiSBA15** treated with HPO_4^{2-} displayed a broad band in the range of 250 to 350 nm (Figure 5, green trace). **TiSBA15** was then treated with both KH_2PO_4 (aq) and H_2O_2 at room temperature for 1 h. A yellow color immediately appeared in the mixture, and the DRUV–vis spectrum displayed the absorption band from 250 to 350 nm, as well as a new band centered around λ_{max} = 354 nm with a tail extending to 500 nm (Figure 5, blue trace). Since this band centered at 354 nm was not observed after treatment of **TiSBA15** with only KH_2PO_4 (aq), it may be attributed to a Ligand to Metal Charge Transfer (LMCT) involving a Ti-OO(H) species. Upon treatment of **TiSBA15** with H_2O_2 and either K_2HPO_4 or $NaHCO_3$, a broad absorption band centered at λ_{max} = 318 nm was observed for each reaction (Supporting Information, Figure S11). Since the K_2HPO_4 (pK_a = 12.7) and the $NaHCO_3$ (pK_a = 10.3) additives result in basic solutions (entries 9 and 6 in Table 1), Ti-OOH species may be deprotonated under these conditions and hence the observed band centered at λ_{max} = 318 nm may be attributed to the formation of Ti(η^2-O_2) species. In summary, these studies suggest that in the presence of $H_2PO_4^-$ and H_2O_2, the active site of the **TiSBA15** material may possess a Ti–O–P heterolinkage as well as a Ti-OO(H) moiety.

Potential Structures Involving the Ti Sites: DFT Studies. Aqueous H_2O_2 degraded only upon contact with the catalysts (vide supra), suggesting that $[Ti \cdot H_2O_2]$ species are initially formed, which can then be converted into an equilibrium mixture of Ti-OOH and/or Ti(η^2-O_2) species in solution (Scheme 1, structures 2, 3, 4). The resulting Ti-OO(H) species are likely responsible for the decomposition of H_2O_2.[17–19] Possible structures of the active Ti-OO(H) species involved in the H_2O_2 decomposition were modeled by DFT methods.

To investigate potential intermediates possessing the Ti-OO(H) moiety, $(HO)Ti[OSi(OH)_3]_3$ (**I**) was chosen as a model compound for **TiSBA15** and optimized at the B3LYP/6-31G(d,p) level in the gas phase. An appropriate model for investigating the reactivity of site-isolated, single-site surface species must contain the constraints inherent to a surface-attached species, while retaining the appropriate "flexibility" associated with known chemical and physical properties.[39] The model system based on the simple X-Ti$[OSi(OH)_3]_3$ fragment is useful for this purpose, since the derivatives of interest minimize to structures with a rigid tris(siloxide)
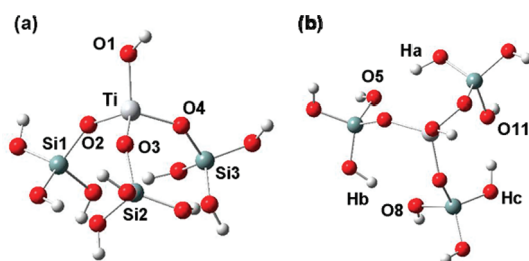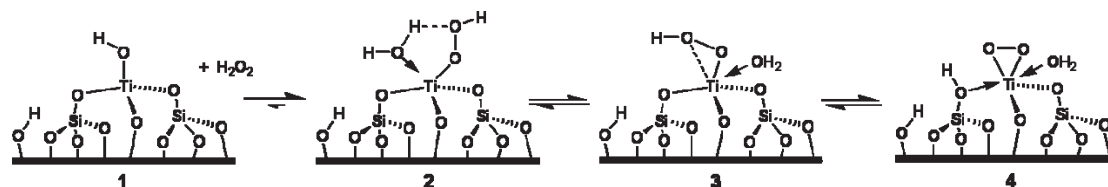
Scheme 1

Figure 6. B3LYP/6-31G(d,p) optimized structure of (HO)Ti[OSi-(OH)$_3$]$_3$ (**I**): (a) side view, and (b) top view. Ti—O1, 1.79 Å; Ti—O2, 1.80 Å; Ti—O3, 1.80 Å; Ti—O4, 1.80 Å; O5-Ha, 1.80 Å; O8-Hb, 1.81 Å; O11-Hc, 1.80 Å.

assembly possessing a hydrogen-bonding network between the three siloxides. These interactions hold the siloxides together and enforce Ti—O—Si bond angles that are close to those expected for a silica-bound Ti center. Further validation of such siloxide-based models for silica-bound, surface titanium species is exhibited by a series of TDDFT calculations (vide infra). In addition, Eisenstein and co-workers have successfully modeled well-defined, silica-supported rhenium metathesis catalysts with use of Ph$_3$SiO- and silsesquioxane ligands for rhenium. These siloxides were shown to provide excellent models to Re—O—Si linkages involving cristobalite and edingtonite surfaces, on the basis of appropriate, comparative calculations.[39] Along these lines, it was shown that structures and energetics of transformations in the -Ti[OSi(OH)$_3$]$_3$ system are very similar to those for analogous derivatives based on the -Ti[O$_{12}$Si$_7$H$_7$] fragment (O$_{12}$Si$_7$H$_7$ = silsesquioxane) (see Supporting Information, Figures S12 and S13).

As depicted in Figure 6, **I** features a tetrahedral environment about Ti with a Ti—OH bond length of 1.79 Å. The Ti—OSi bond lengths are all about 1.80 Å. The calculated Ti—O2—Si1, Ti—O3—Si2, and Ti—O4—Si3 bond angles are 143.8°, 143.8°, and 145.0°, respectively. In addition, three hydrogen bonding interactions are found in **I** (Figure 6b), which may render the optimized complex rather rigid upon modification with H$_2$O$_2$. These interactions result in hydrogen bond distances of 1.80 Å (O5—Ha), 1.81 Å (O8—Hb) and 1.80 Å (O11—Hc).

Reaction of the optimized structure **I** with H$_2$O$_2$ was investigated at the same level of theory, and was found to produce three isomers (**II**, **III**, and **IV**) possessing Ti-OOH or Ti(η^2-O$_2$) moieties. Their relative electronic energies (ΔE's) with respect to **I** + H$_2$O$_2$ were computed at the B3LYP/6-311+G(d,p) level and are listed in Figure 7. The complex (H$_2$O)Ti(η^1-OOH)-[OSi(OH)$_3$]$_3$ (**II**) possess a Ti-hydroperoxo moiety with the calculated bond lengths for Ti—O1 and Ti—O2 of 1.90 Å and 2.94 Å, respectively, indicating that only O1 of the hydroperoxy group is coordinated to Ti. The oxygen atom (O3) from the aquo ligand formed by addition of H$_2$O$_2$ is weakly interacting with Ti (Ti—O3, 2.26 Å), suggesting the presence of dative bonding.
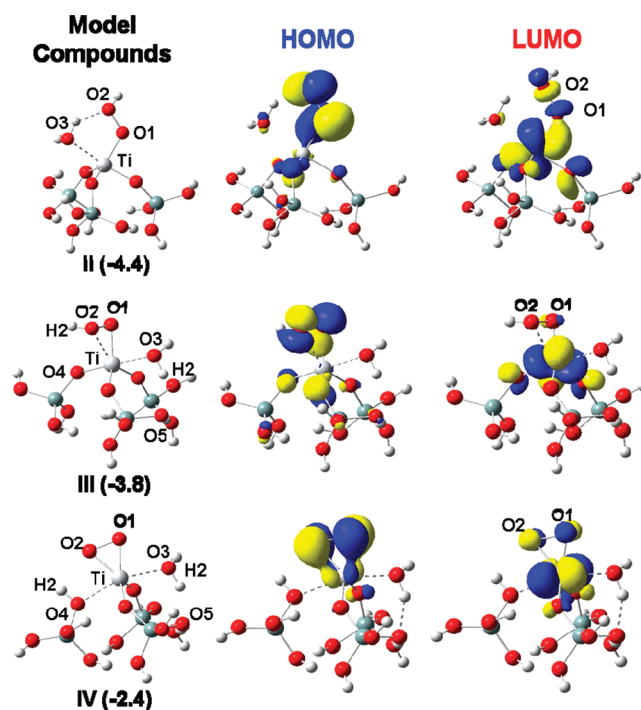

Figure 7. B3LYP/6-31G(d,p) optimized structures and their HOMO and LUMO density surfaces for (H$_2$O)(HOO)Ti[OSi(OH)$_3$]. The relative energies in kcal/mol (parentheses) with respect to **I** + H$_2$O$_2$ were calculated at the B3LYP/6-311+G(d,p) level of theory.

The stabilization energy for this process (**I** + H$_2$O$_2$ → **II**) was calculated to be 4.4 kcal/mol. A second isomer (**III**) possesses the hydroperoxy moiety, which in this case is coordinated to Ti in an η^2 fashion. The Ti—O1 bond length was found to be slightly shorter (1.88 Å) than that in **II**, while the Ti—O2 distance was considerably decreased, to 2.22 Å. In **III**, an additional hydrogen bonding interaction between H2 (of the water ligand) and O5 was found, with a separation of 1.94 Å. The interconversion between **II** and **III** is predicted to be a thermoneutral process (0.60 kcal/mol). Interestingly, the hydrogen atom H2 in **III** is in close proximity to O4 (H2—O4, 2.68 Å) with a O4—Ti—O2—H2 dihedral angle of −8.33°, suggesting that proton transfer from O2 to O4 might readily occur and lead to the formation of a Ti(η^2-O$_2$) species. Indeed, this is the case, and structure **IV** was located with no imaginary frequencies. The Ti—O2 (1.82 Å), H—OSi(OH)$_3$ (H2—O4, 0.97 Å), and Ti—OSi(OH)$_3$ (Ti—O4, 2.27 Å) distances clearly indicate that new bonds between Ti and O2, as well as between H2 and O4, are formed along with breaking of the Ti—O4 bond. Note that O4 interacts with Ti in a dative fashion, and the Ti—O bond lengths involving the peroxo oxygens are identical (Ti—O1, 1.82 Å; Ti—O2, 1.82 Å).

As in **III**, one proton (H2) from the aquo ligand in **IV** interacts with O5 with a separation of 1.77 Å. Structure **IV** was calculated to be 1.4 kcal/mol higher in energy than **III** in the gas phase.

The density surface plots for the highest occupied molecular orbitals (HOMOs) in these structures (Figure 7) illustrate that these orbitals exhibit strong contributions from π-antibonding interactions of the hydroperoxo and peroxo moieties. For structure **IV**, a Ti d orbital also contributes to the HOMO. In contrast, the lowest unoccupied molecular orbitals (LUMOs) associated with these structures are quite different in nature. For **II**, the LUMO is delocalized over the Ti-hydroperoxo moiety, and primarily results from interaction of a Ti-based d orbital with the O–O σ-antibonding orbital. However, the hydroperoxo group in **III** appears to make little contribution to the LUMO. Instead, the LUMO is composed mainly of a d orbital on Ti. For **IV**, the LUMO may be described as involving an antibonding interaction between a Ti d orbital and a π^* orbital of the peroxo group.

■ DISCUSSION

Controlling Factors for H_2O_2 Decomposition. The H_2O_2 decomposition appears to be strongly influenced by both the pK_a and the surface concentrations of the hydroxy groups of the catalytic materials, such that the rates follow the ordering **Bu$_{cap}$TiSBA15** > **TiSBA15** and **TS-1** > **[Ti,Al]-MFI** (Figure 2b). Thus, **Bu$_{cap}$TiSBA15** possesses far fewer surface OH groups than **TiSBA15**, and **[Ti,Al]-MFI** is expected to possess more Brønsted-acidic sites as compared to **TS-1**.[40] Furthermore, since essentially no decomposition was observed after 5 h in water/acetonitrile mixtures without catalysts, or in the presence of only SBA15, the Ti sites are responsible for the H_2O_2 decomposition.

As previously suggested,[5,41-43] the chemisorption of H_2O_2 onto the Ti sites probably generates Ti-OOH species, and this is consistent with the fact that H_2O_2 (pK_a = 11.9) is more acidic than H_2O (pK_a = 15.7).[44] Thus, an important initial process appears to involve a proton-transfer reaction in aqueous solution that results in introduction of a HOO- ligand into the coordination sphere of titanium, probably to produce the previously suggested intermediate involving hydrogen bonding (structure 2, Scheme 1).[5,41-43] This species could exist in equilibrium with other isomers (e.g., structures 3 and 4 in Scheme 1) from which decomposition of O_2 and H_2O follows.

This mechanistic picture suggests that the activation of H_2O_2 on the surface should be sensitive to the Brønsted acidity of the surface hydroxyl groups, since more acidic sites should suppress the deprotonation of H_2O_2, and therefore the formation of intermediate Ti-OOH species involved in the decomposition of H_2O_2. Indeed, as shown in Table 1, the main influence of the inorganic additives appears to be associated with their Brønsted acidity. However, note that whereas KH_2PO_4 and Na_2SO_4 gave solutions of the same initial pH (4–5), the phosphate monobasic salt gave rise to a significantly greater inhibitory effect (for **TiSBA15**). Note that the influence of KH_2PO_4 was not appreciable in the presence of **Bu$_{cap}$TiSBA15**. This minimal inhibitory effect over the hydrophobic **Bu$_{cap}$TiSBA15** material may result from slow diffusion of the $H_2PO_4^-$ anion into the benzene layer in the benzene/aqueous biphasic solution, which suggests that the interactions between Ti and the phosphate additive could be important. Note that in the biphasic mixtures **Bu$_{cap}$TiSBA15** was located at the interface of the benzene-aqueous layers, while the phosphate anion was dissolved in the aqueous layer. Whereas

KH_2PO_4 strongly inhibits the H_2O_2 decomposition rate over **TiSBA15**, this additive has essentially no influence on decompositions catalyzed by **TS-1** and **[Ti,Al]-MFI** (entries 16 vs 18; 21 vs 23). For the dibasic K_2HPO_4 additive, faster decompositions were observed over all Ti-based materials compared to those without this salt, presumably because the additive rendered the solution basic (pH 8–9; entries 9 and 10, 14 and 15, 17 and 18, and 22 and 23).

The observed effects of pH are not surprising because bases are known to promote H_2O_2 decompositions even in the absence of transition metal catalysts. For example, Duke and Haas[45] reported base-catalyzed H_2O_2 decomposition in homogeneous solutions. More recently, Sawyer and co-workers[46] demonstrated the base-induced formation of superoxide from reaction of H_2O_2(aq) and tetrabutylammonium hydroxide in pyridine. The resulting superoxide and hydroxyl radicals led to the formation of molecular oxygen. The influence of acids on H_2O_2 decomposition is also known, and various mineral acids have been used to stabilize H_2O_2.[30,31,47] In addition, Hutchings and co-workers have found that an acid pretreatment of carbon supports for Au/Pd catalysts increases the yield of H_2O_2 production from hydrogen and oxygen.[48] In this context, note that acids could lead to leaching of Ti by protonolysis reactions of Ti–O–Si linkages in the catalytic materials. Thus, it is of great importance to develop efficient catalytic oxidations that prevent the decomposition of H_2O_2 in a range of neutral to slightly acidic conditions. The avoidance of strong acids should also be highly desirable from an environmental point of view. Thus, the KH_2PO_4 additive may be a safe and promising stabilizer for a wide range of oxidations over Ti-based catalysts.

Evidence for the Formation of Ti-OO(H) (Hydroperoxo and/or Peroxo) Species: DRUV–vis Spectroscopic Studies. The interactions between Ti sites and H_2O_2 have been extensively studied for **TS-1** materials,[17,42,43] and on the basis of experimental and computational studies,[17] Ti-OOH and/or Ti(η^2-O_2) intermediates have been proposed (Scheme 1). Although there are still uncertainties concerning structural details, Ti(η^1-OOH) (a) and Ti(η^2-OOH) (b) species (Scheme 1) are widely accepted as active intermediates in oxidation reactions. In contrast, structures containing the Ti(η^2-O_2) moiety (structure 4 in Scheme 1) appear to be inactive for various oxidations.[49-55] For example, Mimoun et al.[49] reported that Ti(η^2-O_2) peroxo titanium complexes (e.g., Ti(OO)($C_6H_4NO_2$)$_2$·OPN$_3C_6H_{18}$) are unreactive toward olefins, allylic alcohols, and cyclic ketones. In addition, it was reported[14] that reaction of the dimeric heteropolycluster ([Bu$_4$N]$_8$[PTiW$_{11}$-O$_{39}$]$_2$O) with H_2O_2 produced the protonated, polyoxometallate (POM) peroxo species ([Bu$_4$N]$_4$[HPTi(OO)W$_{11}O_{39}$]) in which the proton is bonded to phosphorus rather than the Ti(η^2-O_2) moiety. Interestingly, the protonated species exhibited a higher redox potential than a titanium peroxo species ([Bu$_4$N]$_5$[PTi(OO)-W$_{11}O_{39}$]) ($E_{1/2}$ = 1.25 V vs 0.88 V relative to the Ag/AgCl electrode) and is indeed active toward the oxidation of 2,3,6-trimethylphenol, whereas the deprotonated species possessing the Ti(η^2-O_2) moiety was inactive for the same reaction. Very recently, Nomiya and co-workers[56] prepared POMs possessing either Ti(η^2-O_2) or Ti-OOH moieties, and observed that the former peroxo cluster is inactive toward the oxidation of 2-propanol, whereas the latter hydroperoxo species is active toward this oxidation.

The lack of isolable compounds possessing the Ti-OOH group (only one example,[56] vide supra) may be due to the acidic nature of the hydroperoxo ligand bonded to the electron deficient Ti(IV) center. In fact, complexation of the hydroperoxo group

Table 2. Comparisons of Experimental and Simulated λ_{max} Values

	I	II	III	IV
exp.	220	220, 260, 350−450 (broad)[a]		206, 256, 318 (broad)[b]
calc.	215	205, 225, 245, 285 (very small)	210, 230, 250, 275 (very small)	220, 265, 330

[a] λ_{max} of the broad peak could not be obtained. Note that **II** could not be differentiated from **III** experimentally. [b] The generation of **IV** was assumed by the reaction of **TiSBA15** with H_2O_2 in the presence of K_2HPO^4 (pH ~9, Supporting Information, Figure S11).

to a transition metal center is known to lower its pK_a. For example, as compared to a pK_a of 4.7 for free O_2^-, the pK_a of NiO_2^+ is 3.2.[57] The structure of the crystallographically characterized, protonated species $[Bu_4N]_4[HPTi(OO)W_{11}O_{39}]$[14] (vide supra) may also imply an acidic nature for a hydroperoxo ligand attached to an electron-deficient Ti center.

Although little is known regarding homogeneous systems possessing the $Ti(\eta^2\text{-}O_2)$ moiety, efforts to identify the equilibrium between Ti-OOH and $Ti(\eta^2\text{-}O_2)$ in the heterogeneous material, **TS-1**, have been made. Bonino et al.,[58−60] on the basis of DRUV−vis, Raman, and EXAFS/XANES studies, argued that the interconversion between $Ti(\eta^1\text{-}OOH)$ and $Ti(\eta^2\text{-}O_2)$ occurs in the **TS-1**/H_2O_2/H_2O system, with the former hydroperoxo species being colorless while the latter peroxo species is yellow (λ_{max} = 385 nm).

Thus, an important factor in determining the reactivity of a Ti-OOH species generated upon addition of H_2O_2 (aq) to a Ti-based catalyst appears to be its degree of deprotonation under the reaction conditions. DRUV−vis spectroscopy is a useful technique for monitoring the coordination environment about Ti. Utilization of **TiSBA15** provides a convenient way to observe subtle structural changes that result from addition of aqueous H_2O_2 to this material. Thus, a visible (yellow) band appears immediately upon addition of H_2O_2, presumably because the tetrahedral Ti active sites are located on the exterior surface of **TiSBA15**. Compared to the **TiSBA15** material, the visual color change (colorless to yellow) upon addition of H_2O_2 to **Bu$_{cap}$-TiSBA15** was less intense under the same reaction conditions.

An immediate color change to yellow upon treatment of **TiSBA15** with aqueous H_2O_2 may be attributed to the formation of Ti-OO(H) species. Upon addition of potassium phosphate buffer (1 M, pH 8−9) to a mixture of **TiSBA15** and H_2O_2, the yellow color was immediately discharged. Also, the resulting colorless material recovers its yellow color below a pH of about 6, generated by addition of dilute sulfuric acid (10 mM). The absorption (λ_{max}) for the LMCT is dependent upon solution pH (Supporting Information, Figure S14).

In line with the observation by Bonino et al.,[58] the visible band from 300 to 500 nm bleaches upon drying (Figure 4b). The broad, visible band between 300 and 500 nm is also absent after treatment of **TiSBA15** with anhydrous H_2O_2 in CD_2Cl_2. Thus, the observed absorption band centered at λ_{max} = 260 nm may be attributed to the interaction of H_2O_2 with the tetrahedral Ti centers in a η^1 fashion, as proposed previously for **TS-1**.[58] This result is also consistent with those reported by Prestipino et al.,[59] who argue that upon treatment of **TS-1** with anhydrous H_2O_2 vapor, the XANES spectrum is similar to that obtained after dehydration of the **TS-1**/H_2O_2/H_2O system. Moreover, the broad, visible absorption (λ_{max} ~ 330 nm) observed after treatment of **TiSBA15** with H_2O_2 (aq) is again absent after treatment of **TiSBA15** with TBHP in a decane/CH_3CN mixture. Hence, as suggested previously,[58] the role of H_2O appears to be critical for interconversions between $Ti(\eta^1\text{-}OOH)$, $Ti(\eta^2\text{-}OOH)$,
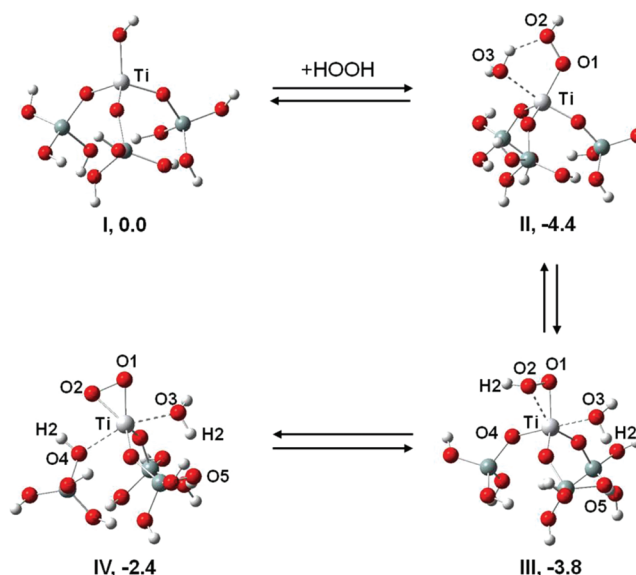

Figure 8. Possible equilibria from the reactions of **I** with H_2O_2. All geometries are optimized at the B3LYP/6-31G(d,p) level. All relative energies ($\Delta E'$s) in parentheses are in kcal/mol. For **II**, Ti−O1, 1.90 Å; Ti−O2, 2.94 Å; Ti−O3, 2.26 Å: For **III**, Ti−O1, 1.88 Å; Ti−O2, 2.22 Å; H2−O4, 2.68 Å; O4−Ti−O2−H2, −8.33°. For **IV**, Ti−O1, 1.82 Å; Ti−O2, 1.82 Å; H2−O4, 0.97 Å; Ti−O4, 2.27 Å.

and $Ti(\eta^2\text{-}O_2)$. These species are likely in equilibrium under aqueous conditions.

To further elucidate the observed species resulting from addition of **TiSBA15** to H_2O_2 (aq), time-dependent DFT (TDDFT) calculations for the optimized geometries of **I**, **II**, **III**, and **IV** were performed with the B3LYP functional in conjunction with the 6-311+G(d,p) basis set. On the basis of the calculated transition energies of singlet excited states and corresponding oscillator strengths, we simulated the absorption spectra of these species and compared them with the experimental results (Table 2). **I** exhibited a sharp transition at λ_{max} = ~220 nm (Supporting Information, Figure S15, a), consistent with previous TDDFT results for the tetrakis(trimethylsiloxy) titanium complex and surface-bound Ti species.[61] The simulated absorption spectra of **II** and **III** (Supporting Information, Figure S15, b and c) are similar to those observed experimentally (Figure 4b, blue trace; Table 2). For the Ti-peroxo species **IV**, a strong absorption at λ_{max} = 330 nm exists in the simulated spectrum (Supporting Information, Figure S15, d), which is in line with the observed spectrum (Supporting Information, Figure S11).

Mechanistic Considerations Addressed with DFT Studies. On the basis of the results described above, along with those previously reported (vide supra), the following hypotheses for the decomposition of H_2O_2 over the Ti(IV)-based materials seem plausible: (1) The Ti species resulting from interaction
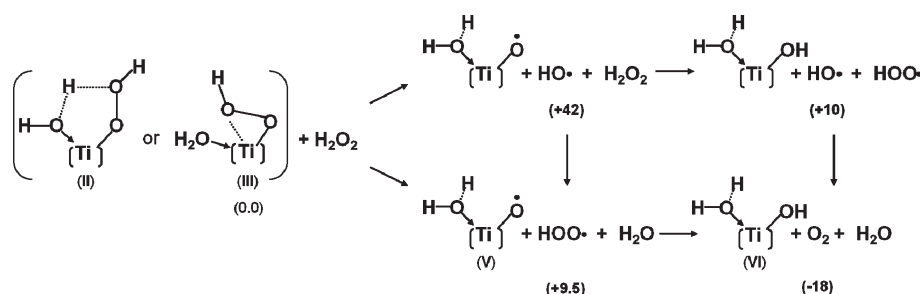
Figure 9. Possible pathways for H_2O_2 decomposition via **II** and **III**. The relative energies (kcal/mol) calculated in the gas phase are in parentheses.
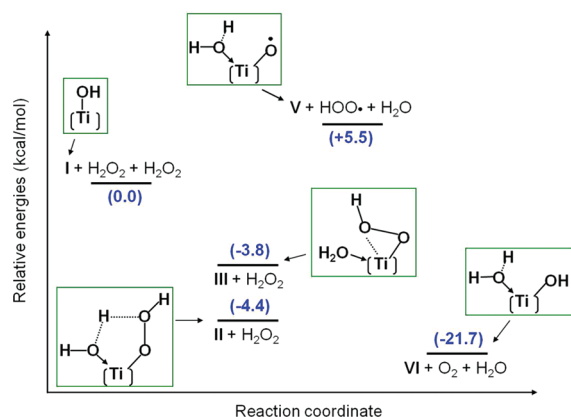

Figure 10. Relative energies for possible intermolecular hydrogen peroxide decomposition pathways via **II** and **III**.
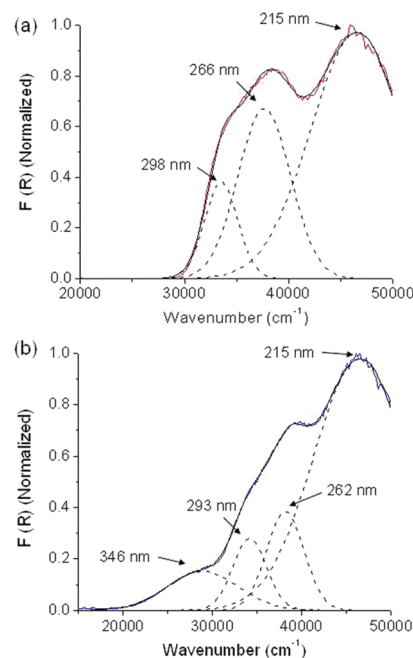

Figure 11. DRUV—vis spectra following (a) treatment of **TiSBA15** with $H_2PO_4^-$; experiment (red); each deconvoluted band (dashed line); a fitted curve based on the deconvoluted bands (solid black), and (b) treatment of **TiSBA15** with both $H_2PO_4^-$ and H_2O_2; experiment (blue); each deconvoluted band (dashed line); a fitted curve based on the deconvoluted bands (solid black). For the analyses, the DRUV—vis spectra (Figure 5, red and blue lines) were rescaled (nm $\rightarrow$ cm^{-1}) and then fitted. In both cases, R^2 values are >0.9995.

with H_2O_2 (model structures for **TiSBA15**; **1**—**4** in Scheme 1) exist in equilibrium in solution and (2) the oxidatively active intermediates $Ti(\eta^1\text{-}OOH)$ (structure **2**) and/or $Ti(\eta^2\text{-}OOH)$ (structure **3**) affect the oxidative decomposition of H_2O_2 (i.e., Ti-OOH is a stronger oxidant than H_2O_2 itself), whereas the oxidatively inert $Ti(\eta^2\text{-}O_2)$ species (structure **4**) may possess a lower oxidizing capability compared to the Ti-OOH species, and hence would not oxidize H_2O_2.

To investigate theses hypotheses, DFT studies were carried out. Previous computational studies have employed $(HO)Ti(OSiH_3)_3$[62] as a model compound to explore mechanisms for epoxidation reactions. Thus, $(HO)Ti(OSiH_3)_3$ was optimized with the B3LYP functional in conjunction with 6-31G(d,p). For comparison, the LANL2DZ effective core pseudopotential for the Ti atom and the 6-31G(d,p) basis set for the silicon, oxygen, and hydrogen atoms were also utilized to optimize the $(HO)Ti(OSiH_3)_3$ model compound. The resulting structure possesses three Ti—O—SiH$_3$ bond angles that are close to 180° (Supporting Information, Figure S16), and this structural feature is most likely a poor representation for the Ti—O—Si heterolinkages present on the surface of the catalysts. In fact, the angles in **TS-1** are predicted to be 140—160° on the basis of EXAFS studies.[17] However, a slightly modified model compound, $(HO)Ti[OSi(OH)_3]_3$ (**I**), optimized at the B3LYP/6-31G(d,p) level, exhibits Ti—O—Si bond angles in the range of 143.8° to 145.0°, in good agreement with those obtained from the EXAFS studies.[17] Moreover, three O—H--O hydrogen bonds between the —Si(OH)$_3$ groups are found to provide a good representation of the rigidity of the silica framework in the heterogeneous **TiSBA15** catalysts (Figure 6). Thus, $(HO)Ti[OSi(OH)_3]_3$ (**I**) was chosen as a model compound to explore possible structures of surface-bound, active Ti species.

To investigate the behavior of possible intermediates **1**—**4** of Scheme 1, the analogous structures **I**—**IV** were optimized, and possible equilibria between these species are depicted in Figure 8. First, because of the more acidic nature of H_2O_2 (p$K_a \sim 9.90$) relative to H_2O (p$K_a = 15.7$), **I** undergoes a proton exchange reaction between H_2O_2 and [Ti]—OH to produce $(H_2O)Ti(\eta^1\text{-}OOH)[OSi(OH)_3]_3$ (**II**) with OOH coordinating to Ti via only one donor atom. This product (**II**) is in equilibrium with **III** (an η^2-OOH complex), in what is predicted to be a thermoneutral process. The proton in the latter hydroperoxo species appears to be quite acidic, as indicated by experimental identification of a deprotonation process that converts **III** to **IV** in aqueous solution (Supporting Information, Figure S14). A transition-state structure responsible for a proton transfer process from **III** to **IV** was located (Supporting Information, Figure S17) and the activation barrier was calculated to be 20.5 kcal/mol in the gas phase

Scheme 2
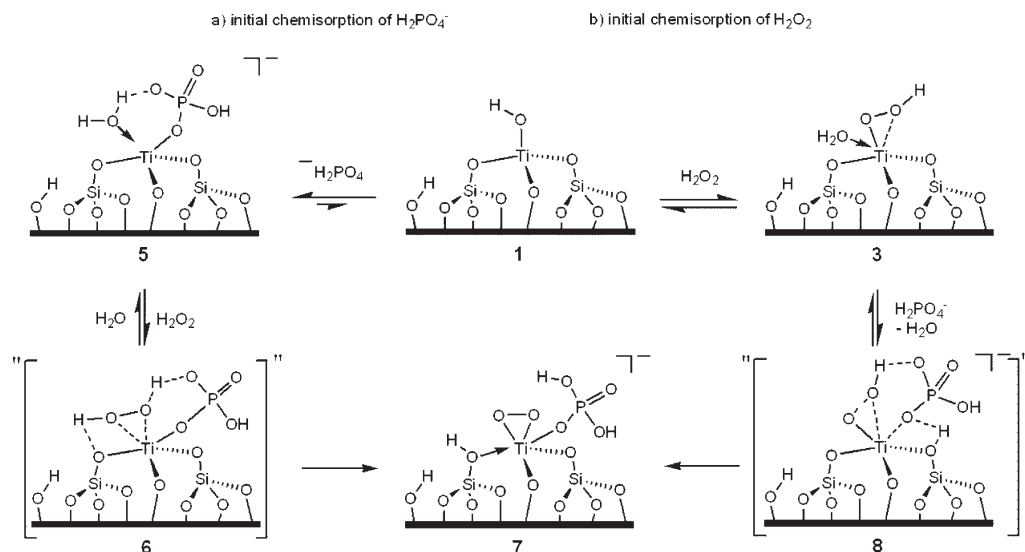
(11.7 kcal/mol in acetonitrile), suggesting that the proton transfer reaction is very likely at 65 °C. Since all calculated ground-state energies in the gas phase as well as in acetonitrile are less than 5.0 kcal/mol (Figure 8), it is conceivable that the Ti-OOH and Ti(η^2-O_2) intermediates **II**—**IV** are in rapid equilibrium in solution.

DFT studies with Ti(η^2-OOH) (**III**) and Ti(η^2-O_2) (**IV**) were extended to explore their relative reactivities in oxidation reactions. Upon reactions of **III** and **IV** with ethylene, oxidization reactions via electrophilic oxygen transfers occur to produce epoxidation products. The gas phase activation energy for the epoxidation with **III** is calculated to be 12.7 kcal/mol, whereas that with **IV** is predicted to be 28.8 kcal/mol (Supporting Information, Figure S18), supporting the hypothesis that titanium peroxo species (**IV**) has a lower oxidizing capability compared to titanium hydroperoxo species **III**. This result is consistent with a previous computational study that reported a kinetic barrier (ca. 10 kcal/mol) for the epoxidation of ethylene with a Ti(OH)(η^2-OOH) species.[63]

Possible oxidative decomposition pathways for H_2O_2 were also considered. Since the radical scavenger BHT slowed down the rate of decomposition (Figure 3 and Supporting Information, Figure S6), it is assumed that a one electron oxidation of H_2O_2 over **II** and/or **III** could occur to produce the hydroperoxy radical (HOO•), which could then be oxidized to produce oxygen.[20] As depicted in Figure 9, **II** or **III** could undergo homolysis of the O—O bond in an intramolecular fashion to generate the hydroxyl radical (HO•), or in an intermolecular manner to oxidize H_2O_2 to the hydroperoxy radical (HOO•). Compared to the high endothermicities (>41 kcal/mol) associated with intramolecular O—O bond homolysis, intermolecular processes are much less endothermic (<10 kcal/mol), suggesting that (H_2O)Ti—O• radical species might be generated from intermolecular reactions of **II** and/or **III** with H_2O_2. The Ti^{IV}—O• radical (**V**) has been previously proposed,[5] and is analogous to V^V—O• radicals that appear to be involved in the hydroxylation of benzene as reported by Bonchio et al.[64] Homolytic Ti—O bond cleavage in Ti(η^2-O_2), to result in formation of a Ti^{III}(η^1-OO•) species, is predicted to be energetically unfavorable (>70 kcal/mol), as calculated at the same level of theory, B3LYP/6-311+G(d,p)//
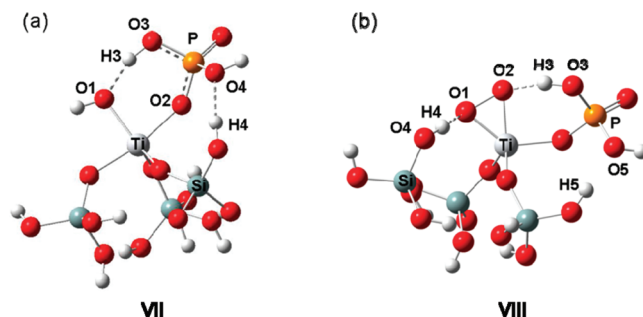

Figure 12. DFT optimized geometries of model compounds (a) **VII** and (b) **VIII** for **5** and **7**, respectively, in Scheme 2. Selected geometrical parameters: For (a), Ti—O1, 1.90 Å; Ti—O2, 1.96 Å; O1—H3, 1.64 Å; H3—O3, 1.00 Å; O4—H4, 1.84 Å; O1—Ti—O2, 84.1°. For (b), Ti—O1, 1.86 Å; Ti—O2, 1.89 Å; O1—O2, 1.47 Å; O2—H3, 1.77 Å; O3—H3, 0.99 Å; O1—H4, 1.82 Å; O4—H4, 0.98 Å; O5—H5, 1.84 Å; O1—Ti—O2, 46.2°; O2—H3—O3, 156°; O1—H4—O4, 164°.

B3LYP/6-31G(d,p). The (H_2O)Ti—O• species produced from homolysis of **II** or **III** could then oxidize HOO• to produce O_2 and the (H_2O)Ti—OH species **VI**, with 27.2 kcal/mol being released. The water bound to Ti in **VI** can be displaced by an additional H_2O_2 molecule to regenerate **II** or **III**, and these processes are calculated to be thermoneutral. For the reaction, **VI** + H_2O_2 → **II** + H_2O, $\Delta E = -0.20$ kcal/mol; for the reaction, **VI** + H_2O_2 → **III** + H_2O, $\Delta E = +0.42$ kcal/mol. The overall exothermicity on going from **I** + 2H_2O_2 to **VI** + O_2 + H_2O is calculated to be 22 kcal/mol (Figure 10). These high thermodynamic driving forces clearly favor the decomposition of H_2O_2 over the catalyst. As can be seen in Figure 10, the intermediate (**V** + HOO• + H_2O) is only 5.5 kcal/mol higher in energy with respect to the reactant (**I** + 2H_2O_2), suggesting that this proposed oxidative decomposition pathway may be energetically feasible.

Molecular orbital analyses support the potential inability of the Ti(η^2-O_2) species **IV** for the H_2O_2 decomposition. Since the Ti-based oxidant should be reduced upon oxidation of H_2O_2, the nature of the LUMO in the Ti species should be relevant.

As depicted in Figure 7, the LUMO of **II** has a strong contribution from the σ^* (O1—O2) orbital, and this should allow the O—O bond to dissociate upon oxidation, to generate a Ti—O$^\bullet$ species and H_2O. For **IV**, a similar electron transfer process from H_2O_2 to the LUMO would presumably not cleave the O1—O2 bond completely, since this orbital has considerable π character (O1—O2 π^*). This interpretation is consistent with the previously reported lower oxidizing power of Ti(η^2-O$_2$) compared to that of Ti-OOH in POMs.[14]

Potential Role of KH$_2$PO$_4$. The observed DRUV—vis spectrum of **TiSBA15** after treatment with $H_2PO_4^-$ was deconvoluted into 3 bands (Figure 11a): (i) a band at λ_{max} = 215 nm, attributed to a $O^{2-} \rightarrow Ti^{4+}$ (T_d) LMCT, (ii) a band centered at λ_{max} = 266 nm that results from expansion of the Ti coordination sphere (e.g., $T_d \rightarrow O_h$, LMCT), and (iii) a band centered at λ_{max} = 298 nm that may correspond to a LMCT from O^{2-}-(phosphate) to Ti^{4+} in a Ti—O—P heterolinkage. The latter band centered at λ_{max} = 298 nm is in line with previous observations for mesoporous Ti phosphate materials that exhibit a broad absorption band from 220 to 330 nm with $\lambda_{max} \sim$ 300 nm.[38] Similarly, the DRUV—vis spectrum of **TiSBA15** following treatment with both $H_2PO_4^-$ and H_2O_2 was deconvoluted into 4 bands (Figure 11b). The absorption bands at λ_{max} = 215, 262, and 293 nm are slightly blue-shifted compared to those of **TiSBA15** after treatment with only KH$_2$PO$_4$. The deconvoluted band centered at λ_{max} = 346 nm may be attributed to the formation of a Ti-OO(H) species, which may further interact with a proton in a phosphate group attached to the Ti center (Figure 11b). For comparison, a Ti(η^2-O$_2$) species formed in the presence of the phosphate dibasic additive K$_2$HPO$_4$ and H_2O_2 exhibited absorption bands centered around λ_{max} = 318 nm (Supporting Information, Figure S19). Thus, the species resulting from treatment of **TiSBA15** with both KH$_2$PO$_4$ and H_2O_2 likely possesses a Ti—O—P heterolinkage as well as a Ti(η^2-O$_2$) or Ti-OO---H$^+$ moiety. Solid-state ^{31}P MAS NMR spectroscopy revealed that a resonance at δ = −2 ppm appeared upon treatment of the **TiSBA15** with KH$_2$PO$_4$. Following treatment of the **TiSBA15** with KH$_2$PO$_4$ and H_2O_2, the resonance at δ = −2 ppm is replaced by a broad peak at about δ = −5 ppm (Supporting Information, Figure S10, a and b). Consistent with the solid-state NMR results, calculated GIAO ^{31}P NMR shifts of **VII** and **VIII** were calculated to be −3.2 and −5.2 ppm, respectively. This suggests a perturbation of the environment about the phosphate ligand, and may correspond to the presence of hydrogen-bonding interactions between an activated hydrogen peroxide species and a phosphate-type ligand. Because of its basic nature (pK_a = 12.7), the presence of the phosphate dianion, HPO$_4^{2-}$ is unlikely, and this is consistent with the observation that the LMCT band centered at λ_{max} = 290 nm and attributed to a Ti—O—P heterolinkage is barely detected upon reaction of **TiSBA15** with the anion (Figure 5, green trace). This spectrum may be deconvoluted into two bands (λ_{max} = 212 and 267 nm respectively, Supporting Information, Figure S20). The species possessing both a Ti—O—P heterolinkage and a partially dissociated Ti-OO---H$^+$ moiety can be independently generated by the initial chemisorption of either $H_2PO_4^-$ or H_2O_2, as outlined in Scheme 2. Similar to the chemisorption of H_2O_2 at the Ti sites, chemisorption of $H_2PO_4^-$ (p$K_a \sim$7.2) onto Ti could produce a 6-membered ring intermediate (**5**; Scheme 2a). Such a structure was optimized at the B3LYP/6-31G(d,p) level with 44 kcal/mol of stabilization energy (**VII**, Figure 12a). Species **5** may then interact with H_2O_2 to produce **7**, presumably via a species such as **6**.

Since siloxide is more basic than the phosphate anion, one of the protons of the Ti(H_2O_2) moiety in **6** may be transferred to a siloxide group, in a process analogous to that of the equilibrium between **3** (and/or **2**) and **4** in Scheme 1. Likewise, **7** can be generated from initial chemisorption of H_2O_2 (Scheme 2b), followed by a chemisorption of $H_2PO_4^-$. An optimized structure **VIII**, a model compound for **7**, was located with an additional hydrogen bonding interaction (O5---H5), as depicted in Figure 12b. In the formation of complex **VIII**, an oxygen atom (O4) is protonated as it moves out of the Ti coordination sphere. A proton (H4) of the new silanol group interacts with an oxygen (O1) in the Ti(η^2-O$_2$) moiety, with the hydrogen bonding interactions among the Si(OH)$_3$ moieties being slightly perturbed. This overall reaction (**I** + $H_2PO_4^-$ + $H_2O_2 \rightarrow$ **VIII** + H_2O) is predicted to be highly exothermic (ΔE = −46 kcal/mol), suggesting that the formation of **7** (**VIII**) is likely in solution. Note that this high exothermicity results mostly from initial chemisorption of $H_2PO_4^-$ to **TiSBA15**; for the reaction, **I** (**1**) + $H_2PO_4^- \rightarrow$ **VII** (**5**), ΔE = −44 kcal/mol, and for the reaction, **VII** (**5**) + $H_2O_2 \rightarrow$ **VIII** (**7**) + H_2O, ΔE = −2.5 kcal/mol. The bond distance between O2 and H3 in **VII** is calculated to be 1.77 Å, which is much shorter than that (2.32 Å) between O2 and H2 found in the deprotonated species **IV**. Thus, **VIII** may be considered as a [Ti-OO---H$^+$] species that is stabilized by hydrogen bonding interactions, and thus may have some Ti-OOH character. Consistent with this interpretation, the TDDFT-predicted spectrum for **VIII** is nearly identical to that (Figure 5d) obtained following treatment of **TiSBA15** with H_2O_2 and KH$_2$PO$_4$, with a strong absorption at $\sim$320 nm (Supporting Information, Figure S21). Since the Ti(η^2-O$_2$) species appear to be inactive for oxidations, formation of the [Ti-OO---H$^+$] species (**7** or **VIII**) may retard H_2O_2 decomposition.

■ CONCLUSIONS

The spectroscopic and DFT investigations described above provide relevant information concerning the mechanism of hydrogen peroxide decomposition, as catalyzed by a titanium center on a silica surface. Extension of these insights to new catalytic systems should prove valuable for maximizing the efficiency of oxidant (H_2O_2) consumption, an issue challenging the development of cost-effective and environmentally friendly catalytic oxidations. This is a particular concern given the potential for a variety of metal centers to activate H_2O_2 for direct decomposition, in addition to the desired substrate oxidation.

Three potential Ti-containing intermediates, Ti(η^1-OOH)-(OH)$_2$, Ti(η^2-OOH)(OH)$_2$, and Ti(η^2-OO)(OH)$_2$, are proposed to exist in equilibrium in an aqueous environment. Interestingly, in contrast to the hydroperoxy species, the latter peroxy complex appears to be relatively inactive in oxidation reactions (toward H_2O_2 and ethylene). Thus, it would seem that acidic conditions might favor titanium-mediated oxidation chemistry, and it is well-known[29] that hydrogen peroxide decomposition is slower under more acidic conditions. However, employing acidic reaction solutions to improve oxidant efficiencies may be problematic, as catalyst degradation (e.g., by leaching) may be accelerated under these conditions. However, for oxidations carried out under conditions near neutral solution pH, catalyst surfaces possessing sufficient surface acidity may lead to improvements in H_2O_2 utilization.

The results from this study strongly suggest that a hydroperoxy-titanium species, formed initially from 1 equiv of H_2O_2, is capable of oxidizing a second equivalent of H_2O_2 to give $^\bullet$OOH

radical and $Ti(O^{\bullet})(OH_2)$ species. Thus, oxidations of organic substrates with H_2O_2 are likely to be more efficient under conditions of low H_2O_2 (and relatively high substrate) concentrations.[65] Along these lines, it has been reported that slow addition of H_2O_2 significantly improves yields for cyclohexene epoxidation.[66,67] In addition, Ladipo and co-workers[15] reported increased epoxide and H_2O_2 selectivities via reduction of local H_2O_2 concentrations at Ti centers, by use of Ti-silsesquioxane complexes within a hydrophobic polydimethylsiloxane (PDMS) membrane.

Finally, a study of the role of inorganic additives on the rate of H_2O_2 decomposition indicates that the phosphate monobasic anion inhibits the decomposition by a mechanism that may not be derived simply from its acid—base properties. On the basis of DRUV—vis spectroscopic and DFT studies, it appears that this stabilization effect may originate from competitive binding to the Ti-center (e.g., $Ti(H_2PO_4)$ formation), and participation of the $H_2PO_4^{2-}$ ligand as a proton-acceptor with formation of a hydrogen-bonded $TiOO\text{---}H(HPO_4)$ complex. Such stabilization effects for H_2O_2 are particularly important for cases in which the additive does not inhibit oxidation of the organic substrate. The $TiOO\text{---}H(HPO_4)$ species may serve as a more efficient oxidant than the hydroperoxy-titanium complexes described above, if it possesses chemical properties that are similar to those of the hydroperoxy (vs the peroxy) titanium species described above. Current investigations indicate that this may be the case for cyclohexene epoxidation, and these results will be reported in the near future.

■ EXPERIMENTAL SECTION

General Information. Unless otherwise noted, all manipulations were performed under an atmosphere of nitrogen using standard Schlenk techniques and/or in a Vacuum Atmospheres drybox. Benzene and acetonitrile were purchased from EM Science and used as received. Aqueous hydrogen peroxide (50 wt %) and *tert*-butyl hydrogen peroxide (TBHP, 5—6 N in decane) were purchased from Aldrich and stored at low temperature (+10 °C). Acetonitrile-d_3 was used as received. Non-aqueous hydrogen peroxide in CD_2Cl_2 was prepared according to the literature procedure.[28] (Dimethyamino)dimethylbutylsilane was purchased from Gelest and stored under inert atmosphere. Tetrapropylammonium hydroxide (40 wt % in water), aluminum hydroxide (55 wt % Al_2O_3), and tetraethyl orthosilicate were used as received from Aldrich. Titanium(IV) butoxide was purchased from Aldrich and stored under inter atmosphere. The following were also prepared according to literature procedures: $HOSi(O^tBu)_3$,[68] $Ti(O^iPr)[OSi(O^tBu)_3]_3$,[26,27] SBA15,[25] TiSBA15,[21] and **Bu$_{cap}$TiSBA15**.[11]

The microporous material **TS-1**[69] was prepared by first mixing tetraethyl orthosilicate (302 g) and titanium(IV) butoxide (6.1 g) in a Teflon beaker under a blanket of nitrogen at room temperature. In a separate Teflon beaker tetrapropylammonium hydroxide (118 g of 40 wt % TPAOH in water) and distilled water (287 g) were mixed. The TPAOH solution was then slowly added to the first solution with stirring at room temperature. An additional loading of distilled water (287 g) was added slowly with stirring until the solution became clear. The resulting solution was then transferred to a series of 125 mL Teflon linears which were placed into 125 mL Parr reactors inside a static oven. The reactors were heated at 160 °C for 96 h, cooled to ambient temperature, and the contents were combined. The pH was adjusted to 8 using 1 M nitric acid, and the mixture was centrifuged

at 7500 rpm for 15 min. The solids were isolated, washed with distilled water, and centrifuged 3 times. The resultant solid was dried at 100 °C for 24 h, and then calcined first under nitrogen and then air. The calcination procedure involved heating to 230 °C under nitrogen at a rate of 1 °C/min, holding for 24 h, then heating to 540 °C at a rate of 1 °C/min, holding for 4 h, and then switching the gas feed to air and holding at 540 °C for 8 h before cooling to ambient temperature. Prior to calcination, a sample was analyzed by X-ray powder diffraction. The resultant spectrum was indicative of an MFI-type lattice.

The microporous material [**Ti,Al**]-**MFI**[70] was prepared by the method described above except that aluminum hydroxide (2.82 g of 50 wt % Al_2O_3) was included within the second addition of distilled water. Prior to calcination, a sample was analyzed by X-ray powder diffraction. The resultant spectrum was indicative of an MFI-type lattice.

Characterization. Solution ^{1}H NMR spectra were recorded at 300 MHz using a Bruker AV-300 spectrometer. Chemical shifts for ^{1}H NMR spectra were referenced internally to the residual solvent proton signal relative to tetramethylsilane. Nitrogen adsorption isotherms were obtained using a Quantachrome Autosorb 1, and samples were outgassed at 120 °C for at least 20 h prior to measurement. The BET method was used to determine surface areas, and the Barrett—Joyner—Halenda (BJH) method was used to obtain pore size distributions. DRUV—vis spectra were obtained using a LabSphere DRA-CA-30I diffuse-reflectance attachment with the Varian-Cary 300 Bio spectrophotometer. MgO was used as the reference background material. Thermal analyses were performed on a TA Instruments SDT 2960 Integrated TGA/DSC analyzer with a heating rate of 10 °C min^{-1} under a flow of nitrogen or oxygen. Following the grafting of the molecular precursor, $Ti(O^iPr)[OSi(O^tBu)_3]_3$, calcinations were performed at 250 °C using a Lindberg three-zone furnace with a heating rate of 10 °C min^{-1} under a flow of oxygen, and the temperature was held constant for 4 h. Titanium elemental analyses were performed at Galbraith Laboratories, Inc. (Knoxville, TN) by ICP methods. Unless otherwise noted, Ti contents in **TiSBA15** and **Bu$_{cap}$TiSBA15** are 2.69 and 1.53 wt % respectively.

Hydrogen Peroxide Decomposition. In a typical experiment using NMR spectroscopy, about 5.0 mg of a desired catalyst was suspended in 0.50 mL of CD_3CN in a J. Young NMR tube. Methylene chloride (5 μL) was added as an internal standard. Hydrogen peroxide (50 μL) was added via syringe at room temperature. The resulting solution was shaken and then placed in a 65 °C oil bath. A ^{1}H NMR spectrum was collected at approximately 1 h intervals over 5 h. The amount of residual hydrogen peroxide was determined via relative peak integration versus methylene chloride (5 μL) as an internal standard.

In a typical batch experiment, a solution containing benzene (1.6 mL), aqueous hydrogen peroxide (50 wt %, 0.4 mL), and acetonitrile (3.2 mL) over **TiSBA15** (5 mg), **Bu$_{cap}$TiSBA15** (8 mg), **TS-1** (8 mg), or [**Ti,Al**]-**MFI** (8 mg) in the presence of either distilled water (1.6 mL) or aqueous solutions (1M, 1.6 mL) containing an additive, was heated at 65 °C for 3 h. The additives were (1) KH_2PO_4, (2) K_2HPO_4, (3) K_3PO_4, (4) KHF_2, (5) $KHSO_4$, (6) Na_2SO_4, (7) $NaHCO_3$, or (8) K_2CO_3. An aliquot (20 μL) was taken, and the amount of residual H_2O_2 was determined after 3 h using standardized $Ce(SO_4)_2$ solutions in the presence of ferroin indicator.

DRUV—vis Spectroscopic Studies. Pellets for the DRUV—vis spectroscopy were prepared according to the following procedure.

For the reaction of **TiSBA15** with aqueous hydrogen peroxide, 0.4 mL of H_2O_2 (aq, 50 wt %) was added to **TiSBA15** (ca. 10 mg), and the resulting mixture was stirred at room temperature for 1 h. The yellow colored solids were then dried under vacuum overnight, and the resulting pale yellow solids were stored under an inert atmosphere. For the reaction of **TiSBA15** with H_3PO_4 (aq), K_2HPO_4 (aq), and KH_2PO_4 (aq), each aqueous solution (3.2 mL) containing the desired phosphate anion was allowed to react with **TiSBA15** (ca. 20 mg) at room temperature for 2 h. The solids were filtered and washed several times with distilled water. The resulting colorless solids were then dried in air overnight. The same procedure described above was used for the reaction of **TiSBA15** with KH_2PO_4 (aq) and H_2O_2 (aq). The resulting yellow solids were dried in air overnight before analysis. For the reaction of **TiSBA15** with TBHP, a solution (3.2 mL) containing TBHP (in decane, 0.1 mL) and CH_3CN (3.2 mL) was added to **TiSBA15** (ca. 29 mg). The resulting mixture was then stirred at room temperature for 1 h. No color change was observed. The colorless solids were filtered, washed several times with CH_3CN, and dried in air. For reactions of **TiSBA15** with H_2O_2 and either K_2HPO_4 or $NaHCO_3$, a solution of K_2HPO_4 (1 M, 3.2 mL) or $NaHCO_3$ (1 M, 3.2 mL) was added to **TiSBA15** and the resulting mixture was stirred at room temperature for 5 min. Aqueous H_2O_2 (50 wt %, 0.4 mL) was then added to this mixture. After stirring the solution at room temperature for 1 h, the solids were isolated by filtration, washed several times with distilled H_2O, and dried in air.

The DRUV—vis spectra following reactions of **TiSBA15** with KH_2PO_4 and both KH_2PO_4 and H_2O_2 were deconvoluted using Gaussian curves to produce Figure 11. The numbers of potential bands in the DRUV—vis spectra obtained experimentally were initially estimated corresponding to visible observation.

Computational Methods. DFT calculations were performed using the Gaussian 03 package.[71] All ground-state and transition-state geometries were fully optimized as gas phase species at the B3LYP/6-31G(d,p) level without any symmetry constraints. Harmonic vibrational analyses were carried out on the optimized geometries at the same level to elucidate the nature of stationary points. True stationary points on the potential energy surface possess no imaginary frequency while true first-order saddle points possess only one imaginary frequency. Intrinsic reaction coordinate (IRC) calculations were carried out in both the forward and reverse directions to confirm the reaction pathways from the located transition states. All DFT energies were computed on the optimized geometries using the B3LYP functional in conjunction with the 6-311+G(d,p) basis set. The zero-point vibrational energies were computed at the B3LYP/6-31G(d,p) level and then scaled.[72] All reported DFT energies are electronic energies with scaled zero-point energy corrections. For radical species, the same level of theory with unrestricted methods were employed to optimize geometries as well as to compute energies at the optimized geometries; that is, all the reported energies were computed at the UB3LYP/6-311+G(d,p)//UB3LYP/6-31G(d,p) level. To consider solvent effects (CH_3CN, $\varepsilon = 35.69$), conductor-like polarizable continuum model (CPCM) was employed with Pauling atomic radii. All energies in CH_3CN were computed at B3LYP/6-311+G(d,p) using the geometries optimized at B3LYP/6-31G(d,p) in the gas phase. TDDFT calculations were carried out at the optimized geometries using the B3LYP functional in conjunction with the 6-311+G(d,p) basis set. GIAO ^{31}P NMR shift calculations were performed at B3LYP/6-311+G(d,p)

employing the optimized geometries of **VII** and **VIII** at B3LYP/6-31G(d,p).

ASSOCIATED CONTENT

Ⓢ **Supporting Information.** The complete list of authors for ref 71. Thermal analyses, DRUV—vis spectra, a NMR spectrum, magic-angle-spinning solid-state ^{31}P NMR spectra, and DFT-optimized geometries, TDDFT results, and their Cartesian coordinates for the Ti-based catalysts. This material is available free of charge via the Internet at http://pubs.acs.org.

AUTHOR INFORMATION

Corresponding Author
*E-mail: tdtilley@berkeley.edu.

Present Addresses
$^{\perp}$The Fuel Cell Center, National Agenda Research Division, Korea Institute of Science and Technology, Seoul, Korea (ROK). $^{\parallel}$Department of Chemistry, University of Rochester, Rochester, NY 14627.

DEDICATION

Dedicated to the memory of Professor Victor Lin.

REFERENCES

(1) Cavani, F.; Teles, J. H. *ChemSusChem* **2009**, *2*, 508–534.

(2) Strukul, G., Ed.; *Catalytic Oxidations with Hydrogen Peroxide as Oxidant*; Kluwer Academic Publishers: Dordrecht, The Netherlands, 1993; Vol. 9.

(3) Salem, I. A.; El-Maazawi, M.; Zaki, A. B. *Int. J. Chem. Kinet.* **2000**, *32*, 643–666.

(4) Sanderson, W. R. *Pure Appl. Chem.* **2000**, *72*, 1289–1304.

(5) Jackson, D. Hargreaves, J. S. J., Eds.; *Metal Oxide Catalysis*; Wiley-VCH: Weinheim, Germany, 2009; Vol. 2, pp 705—749.

(6) Huang, J.; Akita, T.; Faye, J.; Fujitani, T.; Takei, T.; Haruta, M. *Angew. Chem., Int. Ed.* **2009**, *48*, 7862–7866.

(7) Keshavaraja, A.; Ramaswamy, V.; Soni, H. S.; Ramaswamy, A. V.; Ratnasamy, P. *J. Catal.* **1995**, *157*, 501–511.

(8) Balducci, L.; Bianchi, D.; Bortolo, R.; D'Aloisio, R.; Ricci, M.; Tassinari, R.; Ungarelli, R. *Angew. Chem., Int. Ed.* **2003**, *42*, 4937–4940.

(9) Bianchi, D.; Balducci, L.; Bortolo, R.; D'Aloisio, R.; Ricci, M.; Spanò, G.; Tassinari, R.; Tonini, C.; Ungarelli, R. *Adv. Synth. Catal.* **2007**, *349*, 979–986.

(10) Chammingkwan, P.; Hoelderich, W. F.; Mongkhonsi, T.; Kanchanawanichakul, P. *Appl. Catal., A* **2009**, *352*, 1–9.

(11) Brutchey, R. L.; Ruddy, D. A.; Andersen, L. K.; Tilley, T. D. *Langmuir* **2005**, *21*, 9576–9583.

(12) Ruddy, D. A.; Tilley, T. D. *Chem. Commun.* **2007**, 3350–3352.

(13) Ruddy, D. A.; Brutchey, R. L.; Tilley, T. D. *Top. Catal.* **2008**, *48*, 99–106.

(14) Kholdeeva, O. A.; Trubitsina, T. A.; Maksimovskaya, R. I.; Golovin, A. V.; Neiwert, W. A.; Kolesov, B. A.; López, X.; Poblet, J. M. *Inorg. Chem.* **2004**, *43*, 2284–2292.

(15) Aish, E. H.; Crocker, M.; Ladipo, F. T. *J. Catal.* **2010**, *273*, 66–72.

(16) Schuchardt, U.; Cardoso, D.; Sercheli, R.; Pereira, R.; da Cruz, R. S.; Guerreiro, M. C.; Mandelli, D.; Spinacé, E. V.; Pires, E. L. *Appl. Catal., A* **2001**, *211*, 1–17.

(17) Bordiga, S.; Bonino, F.; Damin, A.; Lamberti, C. *Phys. Chem. Chem. Phys.* **2007**, *9*, 4854–4878, and references therein.

(18) Trukhan, N. N.; Romannikov, V. N.; Shmakov, A. N.; Vanina, M. P.; Paukshtis, E. A.; Bukhtiyarov, V. I.; Kriventsov, V. V.; Danilov, I. Yu.; Kholdeeva, O. A. *Microporous Mesoporous Mater.* **2003**, *59*, 73–84.

(19) Fan, W.; Wu, P.; Tatsumi, T. *J. Catal.* **2008**, *256*, 62–73.

(20) Antcliff, K. L.; Murphy, D. M.; Griffiths, E.; Giamello, E. *Phys. Chem. Chem. Phys.* **2003**, *S*, 4306–4316.

(21) Jarupatrakorn, J.; Tilley, T. D. *J. Am. Chem. Soc.* **2002**, *124*, 8380–8388.

(22) Taramasso, M.; Perego, G.; Notari, B. U.S. Patent 4410501, 1983.

(23) Notari, B. *Adv. Catal.* **1996**, *41*, 253–334.

(24) Forni, L.; Pelozzi, M.; Giusti, A.; Fornasari, G.; Millini, R. *J. Catal.* **1990**, *122*, 44–54.

(25) Zhao, D.; Huo, Q.; Feng, J.; Chmelka, B. F.; Stucky, G. D. *J. Am. Chem. Soc.* **1998**, *120*, 6024–6036.

(26) Abe, Y.; Kijima, I. *Bull. Chem. Soc. Jpn.* **1970**, *43*, 466–469.

(27) Gunji, T.; Kasahara, T.; Abe, Y. *J. Sol-Gel Sci. Technol.* **1998**, *13*, 975–979.

(28) Fujdala, K. L.; Tilley, T. D. *J. Am. Chem. Soc.* **2001**, *123*, 10133–10134.

(29) Choudhary, V. R.; Samanta, C.; Jana, P. *Appl. Catal., A* **2007**, *317*, 234–243.

(30) Kakarla, P. K. C.; Watts, R. J. *J. Environ. Eng.-ASCE* **1997**, *123*, 11–17.

(31) Pirault-Roy, L.; Kappenstein, C.; Guérin, M.; Eloirdi, R. *J. Propul. Power* **2002**, *18*, 1235–1241.

(32) Grey, R. A.; Jones, C. A. U.S. Patent 6498259 B1, 2002.

(33) Kaminsky, M. P.; Grey, R. A.; Morales, E. U.S. Patent 0042718 A1, 2009.

(34) Chang, T. U.S. Patent 0306416 A1, 2009.

(35) Marchese, L.; Maschmeyer, T.; Gianotti, E.; Coluccia, S.; Thomas, J. M. *J. Phys. Chem. B* **1997**, *101*, 8836–8838.

(36) Brutchey, R. L.; Mork, B. V.; Sirbuly, D. J.; Yang, P.; Tilley, T. D. *J. Mol. Catal. A* **2005**, *238*, 1–12.

(37) DiPasquale, A. G.; Mayer., J. M. *J. Am. Chem. Soc.* **2008**, *130*, 1812–1813.

(38) Bhaumik, A.; Inagaki, S. *J. Am. Chem. Soc.* **2001**, *123*, 691–696.

(39) Solans-Monfort, X.; Filhol, J.-S.; Copéret, C.; Eisenstein, O. *New J. Chem.* **2006**, *30*, 842–850.

(40) Thangaraj, A.; Kumar, R.; Sivasanker, S. *Zeolite* **1992**, *12*, 135–137.

(41) Clerici, M. G. *Appl. Catal.* **1991**, *68*, 249–261.

(42) Clerici, M. G.; Ingallina, P. *J. Catal.* **1993**, *140*, 71–83.

(43) Bellussi, G.; Carati, A.; Clerici, M. G.; Maddinelli, G.; Millini, R. *J. Catal.* **1992**, *133*, 220–230.

(44) Streitwieser, A.; Heathcock, C. H.; Kosower, E. M. *Introduction to Organic Chemistry*, 4th ed.; Macmillan Publishing Company: New York, 1992; p 67.

(45) Duke, F. R.; Haas, T. W. *J. Phys. Chem.* **1961**, *65*, 304–306.

(46) Roberts, J. L., Jr.; Morrison, M. M.; Sawyer, D. T. *J. Am. Chem. Soc.* **1978**, *100*, 329–330.

(47) Kaale, E. A.; Haule, A. F.; Mung'ong'o, S.; Kishiwa, M. *J. Clin. Pharm. Ther.* **2007**, *32*, 613–616.

(48) Edwards, J. K.; Solsona, B.; Ntainjua, E.; Carley, A. F.; Herzing, A. A.; Kiely, C. J.; Hutchings, G. J. *Science* **2009**, *323*, 1037–1041.

(49) Mimoun, H.; Postel, M.; Casabianca, F.; Fischer, J.; Mitschler, A. *Inorg. Chem.* **1982**, *21*, 1303–1306.

(50) Ledon, H. J.; Varescon, F. *Inorg. Chem.* **1984**, *23*, 2735–2737.

(51) Yamase, T.; Ishikawa, E.; Asai, Y.; Kanai, S. *J. Mol. Catal. A: Chem.* **1996**, *114*, 237–245.

(52) Postel, M.; Casabianca, F.; Gauffreteau, Y.; Fischer, J. *Inorg. Chim. Acta* **1986**, *113*, 173–180.

(53) Sisemore, M. F.; Selke, M.; Burstyn, J. N.; Valentine, J. S. *Inorg. Chem.* **1997**, *36*, 979–984.

(54) Yamase, T.; Ozeki, T.; Motomura, S. *Bull. Chem. Soc. Jpn.* **1992**, *65*, 1453–1459.

(55) Sakai, Y.; Kitakoga, Y.; Hayashi, K.; Yoza, K.; Nomiya, K. *Eur. J. Inorg. Chem.* **2004**, 4646–4652.

(56) Hayashi, K.; Kato, C. N.; Shinohara, A.; Sakai, Y.; Nomiya, K. *J. Mol. Catal. A: Chem.* **2007**, *262*, 30–35.

(57) Sellers, R. M.; Simic, M. G. *J. Am. Chem. Soc.* **1976**, *98*, 6145–6150.

(58) Bonino, F.; Damin, A.; Ricchiardi, G.; Ricci, M.; Spanò, G.; D'Aloisio, R.; Zecchina, A.; Lamberti, C.; Prestipino, C.; Bordiga, S. *J. Phys. Chem. B* **2004**, *108*, 3573–3583.

(59) Prestipino, C.; Bonino, F.; Usseglio, S.; Damin, A.; Tasso, A.; Clerici, M. G.; Bordiga, S.; D'Acapito, F.; Zecchina, A.; Lamberti, C. *ChemPhysChem* **2004**, *5*, 1799–1804.

(60) Bordiga, S.; Damin, A.; Bonino, F.; Ricchiardi, G.; Lamberti, C.; Zecchina, A. *Angew. Chem., Int. Ed.* **2002**, *41*, 4734–4737.

(61) O'Shea, V. A. D.; Capel-Sachez, M.; Blanco-Brieva, G.; Campos-Martin, J. M.; Fierro, J. L. G. *Angew. Chem., Int. Ed.* **2003**, *42*, 5851–5854.

(62) Neurock, M.; Manzer, L. E. *Chem. Commun.* **1996**, 1133–1134.

(63) Sinclair, P. E.; Catlow, R. A. *J. Phys. Chem. B* **1999**, *103*, 1084–1095.

(64) Bonchio, M.; Conte, V.; Furia, F. D.; Modena, G. *J. Org. Chem.* **1989**, *54*, 4368–4371.

(65) Future investigations will involve kinetic studies to further address this issue.

(66) Fraile, J. M.; García, J. I.; Mayoral, J. A.; Vispe, E. *Appl. Catal., A* **2003**, *245*, 363–376.

(67) Guidotti, M.; Pirovano, C.; Ravasio, N.; Lázaro, B.; Fraile, J. M.; Mayoral, J. A.; Coq, B.; Galarneau, A. *Green Chem.* **2009**, *11*, 1421–1427.

(68) Abe, Y.; Kijima, I. *Bull. Chem. Soc. Jpn.* **1969**, *42*, 1118.

(69) Thangaraj, A.; Eapen, M. J.; Sivasanker, S.; Ratnasamy, P. *Zeolites* **1992**, *12*, 943–950.

(70) Ovejero, G.; Grieken, R.; van; Uguina, M. A.; Serrano, D. P.; Melero, J. A. *J. Mater. Chem.* **1998**, *8*, 2269–2276.

(71) Frisch, M. J. et al. *Gaussian 03*, Revision C.02; Gaussian, Inc.: Wallingford, CT, 2004; see Supporting Information for complete author list.

(72) Nosenko, Y.; Thummel., R. P.; Mordzinski, A. *Phys. Chem. Chem. Phys.* **2004**, *6*, 363–367.